2D Materials

PAPER

Second Harmonic Generation in WSe_2

RECEIVED
28 August 2015

REVISED
21 October 2015

ACCEPTED FOR PUBLICATION
3 November 2015

PUBLISHED
16 December 2015

J Ribeiro-Soares[1,2,3,11], C Janisch[4,5,11], Z Liu[4,5], A L Elías[5,6], M S Dresselhaus[2,7], M Terrones[5,6,8,9,10], L G Cançado[1] and A Jorio[1]

[1] Departamento de Física, Universidade Federal de Minas Gerais, Belo Horizonte, MG, 30123-970, Brazil
[2] Department of Electrical Engineering and Computer Science, Massachusetts Institute of Technology (MIT), Cambridge, MA 02139, USA
[3] Departamento de Física, Universidade Federal de Lavras, Lavras, MG, 37200-000, Brazil
[4] Department of Electrical Engineering, The Pennsylvania State University, University Park, Pennsylvania 16802, USA
[5] Center for 2-Dimensional and Layered Materials, The Pennsylvania State University, University Park, Pennsylvania 16802, USA
[6] Department of Physics, The Pennsylvania State University, 104 Davey Laboratory, University Park, PA 16802, USA
[7] Department of Physics, Massachusetts Institute of Technology (MIT), Cambridge, MA 02139, USA
[8] Department of Chemistry, The Pennsylvania State University, University Park, PA 16802, USA
[9] Department of Materials Science and Engineering, The Pennsylvania State University, University Park, PA 16802, USA
[10] Research Center for Exotic Nanocarbons (JST), Shinshu University, Wakasato 4-17-1, Nagano, 380-8553, Japan
[11] These authors contributed equally to this work

E-mail: jenaina.soares@dfi.ufla.br

Keywords: transition metal dichalcogenides, second harmonic generation, Raman spectroscopy, photoluminescence

Abstract

Second harmonic generation of single- and few-layer mechanically exfoliated tungsten diselenide (WSe_2) samples are studied. The value of the effective second-order nonlinear susceptibility for monolayer WSe_2 is obtained, being three orders of magnitude larger than the values usually reported for other nonlinear bulk crystals. The presence of a monolayer is certified by symmetry analysis of the Raman modes and the occurrence of a direct band gap. Our results on WSe_2 solidify the family of transition metal dichalcogenides as two-dimensional systems with ultra high second-order nonlinear susceptibility.

1. Introduction

The class of layered transition metal dichalcogenides (TMDs) is presently attracting increased attention due to the observation of new physical phenomena arising in systems of reduced dimensionality [1–3]. Both the discovery of special optical and electrical properties, as well as new application possibilities, have multiplied in recent studies on TMD materials exfoliated down to films of monolayer thickness. The monolayer version is composed of one transition metal atom (*M*) and two chalcogen atoms (*X*), in the form *X*-*M*-X or MX_2. This is, in fact, an atomic trilayer (TL) in which the two principal coordinations for the metal atoms are trigonal prismatic (2*H*) and octahedral (1*T*) [4, 5]. The bulk form of some TMDs, such as MoS_2, WS_2, and WSe_2, are indirect gap semiconductors, but an indirect-to-direct gap transition is observed when decreasing the number of layers down to a monolayer (one that is TL) [1, 6–10], making these materials suitable for optoelectronic applications and complementing graphene (which is gapless) in device fabrication.

The second harmonic generation (SHG) technique has been used to probe symmetry variations, i.e., the presence or absence of inversion symmetry in different types of TMDs [11–15]. While an extensive list of nonlinear crystal second-order susceptibility values can be found in the related literature [16–18], the exploitation of nonlinear optical properties of few-layer nanomaterials is in its beginning. Most impressive is the enhancement of the nonlinear optical properties of TMDs when decreasing the number of layers. The second-order nonlinear susceptibility in MoS_2 increases from values on the order of 10^{-5} nm/V in bulk form to 5 nm/V (see table 1) in the MoS_2 monolayer [13]. The WS_2 monolayer exhibits a similar high second-order susceptibility (see table 1) [19]. A recent work showed that the SH emission of monolayer WSe_2 at a low temperature ($T = 4$ K) can be enhanced (up to 3 orders of magnitude) when using laser excitation in exciton resonances at 1.75 and 2.17 eV [20]. In this work, we perform SHG analysis in mono- and few-layer WSe_2 at ambient temperature and for a single excitation wavelength. Raman spectroscopy and photoluminescence measurements are used to verify the

© 2015 IOP Publishing Ltd

Table 1. Values of the second-order nonlinear susceptibility d (nm/V) for one TL (2D) and bulk (3D) TMDs and for common nonlinear crystals found in the literature. *H* and *R* indicate trigonal prismatic and rhombohedral stackings, respectively. The 9 L corresponds to nine layers of GaSe. Also indicated is the laser wavelength λ_L (nm) used for each experiment.

Materials	d (nm/V)	λ_L (nm)	References
H(one TL) WSe_2	$d_{eff} = 5$	816	This work
H(one TL) MoS_2	$d_{eff} = 5$	810	[13]
H(one TL) WS_2	$d_{eff} = 4.5$	832	[19]
3*R* MoS_2 (bulk)	$d_{21} = 0.5$	1064	[21]
GaAs	$d_{14} = 368.7 \times 10^{-3}$	10 600	[16]
GaSe	$d_{22} = 54.4 \times 10^{-3}$	10 600	[16]
(9L) GaSe	$d_{eff} = 9.3 \times 10^{-3}$	1560	[22]
β-BaB_2O_4	$d_{11} = 1.6 \times 10^{-3}$	1064	[16]
	$d_{22} = 2.2 \times 10^{-3}$	1064	[16]
	$d_{31} = 0.16 \times 10^{-3}$	1064	[16]
α-SiO_2 (quartz)	$d_{11} = 0.4 \times 10^{-3}$	1058.2	[17]
2*H* (bulk) MoS_2	$d_{eff} < 5 \times 10^{-5}$	1064	[21]

presence of monolayer WSe_2. The results characterize a monolayer sample with an estimated nonlinear susceptibility value of d_{eff} ~ 5 nm/V (at 816 nm excitation), which is at least 3 orders of magnitude larger than that of usual nonlinear crystals. The results obtained here add another material to the family of two-dimensional (2D) TMD systems demonstrating ultrahigh second-order nonlinear susceptibility.

2. Results and discussion

Sample description. WSe_2 single crystals were synthesized using chemical vapor transport, following the established method reported in [23]. Few-layer samples were deposited on top of a 300 nm SiO_2/Si substrate using the scotch tape mechanical exfoliation method [24]. Figure 1(a) shows an optical image of a few-layer sample of WSe_2 where one, two and three TLs and bulk (in white) are indicated. The number of TLs is determined by combining the optical, photoluminescence, and Raman spectroscopy data.

Raman spectroscopy. Raman measurements were performed using a Renishaw InVia spectrometer equipped with a Leica microscope with a 50× objective (in the backscattering configuration) using 514 nm laser excitation. The laser power used to acquire these spectra was 35 μW for few-layer samples and 400 μW for bulk samples (to avoid laser damage of the samples [24]), taking two accumulations of 60 s for each spectrum. Raman spectra are plotted in figure 1(b).

The main first-order features of the Raman spectrum of WSe_2 bulk samples are the Raman active E_{1g}, E^1_{2g}, E^2_{2g}, and A_{1g} modes with frequencies at 178, 250, 25 and 253 cm^{-1}, respectively [25]. The E_{1g} mode is symmetry forbidden in the Raman backscattering configuration, while the low frequency E^2_{2g} is too close to the Rayleigh line and, therefore, not observable in our setup. In few-layer WSe_2, the main features observed in figure 1(b) are the peaks at ~250, ~260, and ~310 cm^{-1}. Both E^1_{2g} and A_{1g} modes contribute to the peak at 250 cm^{-1} [26, 27]. The mode at 260 cm^{-1} was identified as a second-order Raman peak [8, 23, 28]. The peak at ~310 cm^{-1} is not Raman active for one TL WSe_2 (as seen in the bottom spectrum of figure 1(b)), but it becomes active for a larger number of layers ($N > 1$). The activation of this mode in Raman scattering spectra of NTL WSe_2 ($N > 1$) is due to the breakdown of the translational symmetry along the '*c*' axis (the axis perpendicular to the basal plane of the TLs). Therefore, the absence of the Raman peak at ~310 cm^{-1} for the sample region marked with one TL (see figure 1(a) and the bottom spectrum in figure 1(b)) is an indication of single-layer WSe_2.

Photoluminescence analysis. Figure 1(c) shows a luminescence image in which the brightest regions indicate a larger intensity luminescence signal. The image was acquired with an Imager A2m Zeiss microscope using laser excitation at 560 nm with a 50 × objective and equipped with an AxioCam MRm camera. The photoluminescence spectra in figure 1(d) was acquired with a Leica microscope using a 50 × objective and 488 nm laser excitation in the backscattering configuration. Extended mode acquisition was used with one acquisition of 10 s, while using a laser power of 16 μW at the sample surface. The regions of one TL, two TLs, three TLs, and bulk WSe_2 are indicated and, as the number of TLs increases, the luminescence contrast diminishes. Figure 1(d) illustrates the remarkable difference between the photoluminescence signal from the one TL and from the bulk regions. The main feature of one TL in figure 1(d) is due to the direct transition that occurs between the valence and the conduction bands at the *K* point of the Brillouin zone.

Second harmonic generation. Figure 1(e) shows the SH image obtained by a raster scan of the few-layer WSe_2 sample. A Ti:sapphire laser (KM Labs) with a central wavelength at 816 nm and a repetition rate of 88 MHz was focused on the sample through a long working distance objective lens (Mitutoyo 50 ×, numerical aperture (NA) = 0.55). The schematics of the homemade SHG microscope is shown in [19, 29]. The SH signal was collected through the same objective lens and was detected by a spectrometer (PI Action 2500i with a liquid nitrogen cooled charge coupled device camera). The contrast in figure 1(e) shows that the one TL location yields an intense SH signal, while the signal from three TLs is less intense but still comparable to that of one TL. The two TL region of the sample does not show a measurable signal. The bulk region of the sample, however, shows some observable SH signal. The SHG of the SiO_2/Si substrate is not substantial for this measurement (SiO_2/Si has been

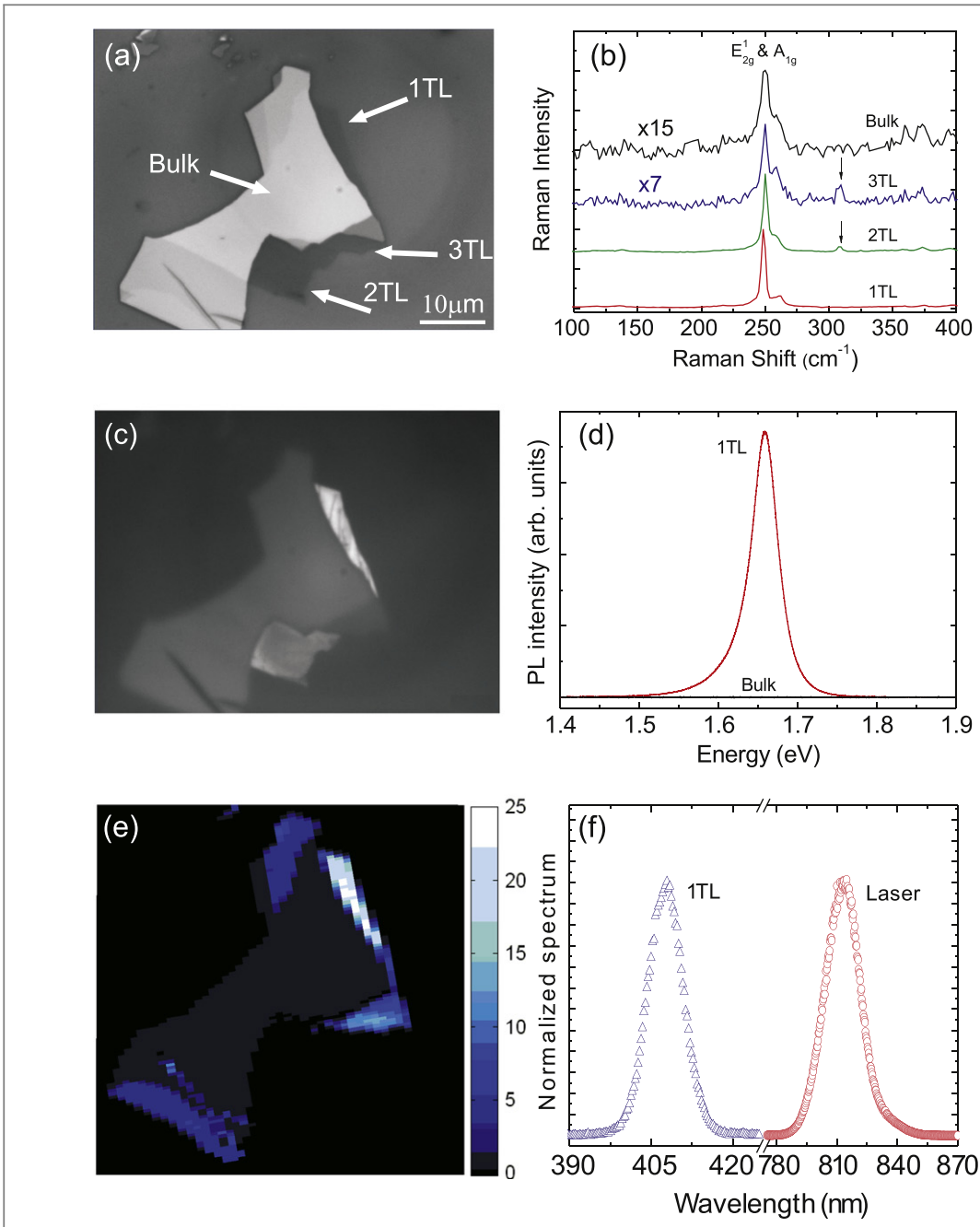

Figure 1. Optical characterization of a WSe_2 mechanically exfoliated sample sitting on top of a 300 nm SiO_2/Si substrate. (*a*) Optical image. The number of TLs in each region as well as in the bulk area are indicated. (*b*) Raman spectra of one, two, and three TL samples, as well as of the bulk sample shown in (*a*). The spectra of the three TLs and bulk samples were multiplied by factors of 7 and 15, respectively, for clarity. (*c*) Luminescence image from the same WSe_2 sample as shown in (*a*). (*d*) Photoluminescence spectra acquired from the one TL WSe_2 and from the bulk WSe_2. (*e*) A SH image from the same WSe_2 sample. (*f*) SH spectrum for WSe_2 one TL (blue), and the fundamental laser spectrum (red). The pump laser is attenuated to show the unsaturated spectrum.

reported previously to show no significant SH signal in comparison to that from suspended samples [19]). Also, the SiO_2/Si substrate can modify the SHG signal due to cavity effects in the SiO_2 layer between the monolayer and the Si substrate, causing the SHG to be overestimated by ~10% [29].

The presence (or absence) of a SHG signal is a fundamental consequence of the absence (presence) of inversion symmetry in crystals under the dipole approximation [17, 18]. The inversion symmetry is broken for an odd number of layers (in this case, the one TL and three TLs). An odd number of layers belongs to the D^1_{3h} space group (which lacks the inversion symmetry operation), and thus the one TL and three TL samples show an intense SH signal (see figure 1(e)). For the even number of layers, WSe_2 belongs to the D^3_{3d} space group, the inversion symmetry operation is present and, as a consequence, two TL WSe_2 does not show SHG. This is a powerful symmetry argument since it probes the inversion symmetry based on SHG considerations. For example, the one T-WSe_2 (WSe_2 in which the transition metal W

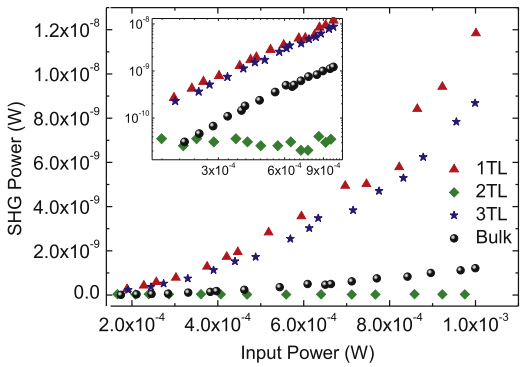

Figure 2. Plot of the SHG signal power as a function of the input power for the regions indicated in figure 1(e). The inset shows the same data on a logarithmic scale.

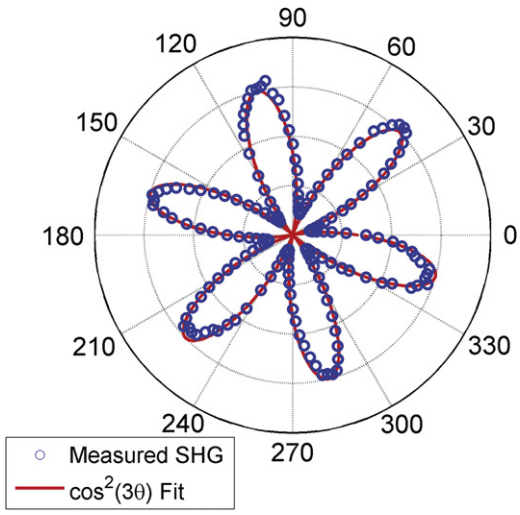

Figure 3. Polarized SHG response of the WSe_2 monolayer. Blue circles represent the measured SHG signal at the rotated polarization. The solid red curve represents the theoretical $\cos^2(3\theta)$ plot.

atoms have octahedral coordination with the chalcogen Se atoms [4, 5]) must show no SHG since both N-odd and N-even few layers belong to the space group for which the inversion symmetry is present [5, 26].

Figure 1(f) shows the SH spectrum of the WSe_2 one TL (blue) and the fundamental laser spectrum (in red), showing the frequency doubling effect. Since the SHG is a nonlinear second-order process, the SH signal intensity is a quadratic function of the input laser intensity. To verify whether or not the emission observed in the bright regions is due to a genuine SH signal, we plot the quadratic dependence, as shown in figure 2, relating the detected average SHG power (P_{SHG}) and the input average power (P_{input}). The inset in figure 2 with a logarithmic scale shows a quadratic power dependence. The linear fit of the form $\log(P_{\mathrm{SHG}}) = a + b \cdot \log(P_{\mathrm{input}})$ gives the coefficient $b = (2.18 \pm 0.04)$ for one TL, (2.18 ± 0.03) for three TLs, and (2.33 ± 0.05) for a bulk specimen. These values confirm the observation of SHG for $N = 1, 3$, where N denotes the number of layers.

Using the approach previously outlined in [19], the SHG signal is calculated using the Green's function of a nonlinear sheet source. In our theoretical model, a fundamental plane wave beam is focused by an objective lens to pump the WSe_2 sheet, generating a SHG signal. This SHG signal is epicollected by the same lens. The SHG signal generated by the semi-infinite substrate is ignored, which is justified by the negligible SHG power collected from the substrate (figure 1(e)). The surface second-order nonlinear susceptibility $\chi_s^{(2)}$ can be estimated in terms of the average power P_i ($i = 1$ for the fundamental and $i = 2$ for the SH pulse), the pulse repetition rate ($R = 88$ MHz), pulse width ($t = 107$ fs), and wavelength ($\lambda_1 = 816$ nm for the fundamental and $\lambda_2 = 408$ nm for the SH frequency), the refractive index n_i ($n_1 = 1.45$ for the refractive index of the substrate at λ_1, and $n_2 = 1.46$, for λ_2) and the numerical aperture (NA) of the lens (NA = 0.55),

$$\chi_s^{(2)} = \sqrt{\frac{\epsilon_0 c \lambda_2^4 P_2 R t_1^2 \left(n_2 + 1\right)^2 \left(n_1 + 1\right)^4}{32\,(\mathrm{NA})^2 t_2 P_1^2 \varphi}}, \qquad (1)$$

where

$\varphi = 8\pi \int_0^1 |\cos^{-1}\rho - \rho\sqrt{1-\rho^2}\,|^2 \rho\, \mathrm{d}\rho \approx 3.53$ [19]. The effective bulk-like second-order susceptibility (d_{eff}) is calculated using the relation $d_{\mathrm{eff}} = \chi_s^{(2)}/2T$, where T is the thickness of the one TL WSe_2 ($T = 0.7$ nm), and $\mathrm{d_{eff}} \cong 5$ nm/V is obtained for a WSe_2 monolayer. For WS_2 one TL, $\mathrm{d_{eff}} \cong 4.5$ nm/V ($T = 0.65$ nm) [19]. Due to the intense nonlinear response, it was possible to observe the SH signal for an input average power as low as 0.2 mW.

The polarization dependence of the SHG signal is sensitive to crystal orientation and reveals the crystal symmetry. The polar plot of the SHG intensity of monolayer WSe_2 is shown in figure 3. In this experiment, the polarization of the incident light was rotated while the sample was kept in its position. For monolayer WSe_2 (D_{3h}^1 space group), the nonzero elements of the second-order nonlinear susceptibility tensor are $\mathrm{d}_{xxx} = -\mathrm{d}_{xyy} = -\mathrm{d}_{yyx} = -\mathrm{d}_{yxy}$ (x is the armchair direction, and y is the zigzag direction). This leads to a polarized SHG power distribution proportional to $\cos^2(3\theta)$ as can be seen in figure 3. One important aspect to be emphasized when working with new 2D materials is the crystallographic orientation of the crystal. In particular, for 2D heterostructures and for strain engineering and applications that are dependent on the edge atomic structure, the properties under scrutiny can be anisotropic [30, 31], and SHG measurements provide a reliable technique to find the crystal orientation in samples that do not have inversion symmetry.

In [20], low temperature ($T = 4$ K) and multiple wavelengths (from 1.7 to 2.4 eV) were used to acquire data for monolayer WSe_2 in which variations of 3

orders of magnitude in SHG intensity were detected at exciton resonances. The SHG measurements acquired in the present work were performed using a single wavelength and outside the range addressed by [20]. From this fact, it is possible that even higher values of d_{eff} can be found when resonance conditions are achieved as a result of probing the laser energy dependence. A similar situation was found in [19], in which calculations of the nonlinear susceptibility of monolayer WS_2 as a function of photon energy predicted resonance effects.

3. Summary

To summarize, table 1 shows the values of the second-order nonlinear susceptibility (d_{eff}) found for some TMDs showing one TL regions, including the value of d_{eff} for WSe_2 reported in the present work. The d_{eff} values for one TL WSe_2 are three orders of magnitude larger than that for commonly used nonlinear crystals. Raman spectroscopy and photoluminescence were used to support the sample identification. The effective second-order nonlinear susceptibility value of $d_{\text{eff}} \sim 5$ nm/V was obtained for monolayer WSe_2. The reduced thickness of one TL WSe_2 together with its high SHG opens the possibility of using one TL TMDs for highly efficient and dimension-reduced nonlinear devices [29].

Acknowledgments

JRS acknowledges the support from the Brazilian Conselho Nacional de Desenvolvimento Cientfico e Tecnolgico (CNPq) under Grant No. 551953/2011-0. MSD and JRS acknowledge financial support from the National Science Foundation under Grant No. DMR-1004147. AJ acknowledges financial support from the Brazilian Conselho Nacional de Desenvolvimento Cientfico e Tecnolgico (CNPq) under Grant No. 552124/2011-7. LGC acknowledges the support from the Brazilian agencies National Counsel of Technological and Scientific Development (CNPq) and Fundação de Amparo a Pesquisa do Estado de Minas Gerais (FAPEMIG). ZL and ALE acknowledge the support from the National Science Foundation under Grant No. EFRI-1433311. MT and ALE acknowledge the U.S. Army Research Office MURI Grant No. W911NF-11-1 − 0362 and the National Science Foundation (2*DARE* − *EFRI* − 51372131).

References

[1] Wang Q H, Kalantar-Zadeh K, Kis A, Coleman J N and Strano M S 2012 Electronics and optoelectronics of two-dimensional transition metal dichalcogenides *Nat. Nanotechnology* **7** 699–712

[2] Chhowalla M, Shin H S, Eda G, Li L J, Loh K P and Zhang H 2013 The chemistry of two-dimensional layered transition metal dichalcogenide nanosheets *Nat. Chem.* **5** 263–75

[3] Butler S Z *et al* 2013 Progress, challenges, and opportunities in two-dimensional materials beyond graphene *ACS Nano* **7** 2898–926

[4] Wilson J A and Yoffe A D 1969 The transition metal dichalcogenides discussion and interpretation of the observed optical, electrical and structural properties *Adv. Phys.* **18** 193–335

[5] Ribeiro-Soares J, Almeida R M, Barros E B, Araujo P T, Dresselhaus M S, Cançado L G and Jorio A 2014 Group theory analysis of phonons in two-dimensional transition metal dichalcogenides *Phys. Rev.* B **90** 115438

[6] Splendiani A, Sun L, Zhang Y, Li T, Kim J, Chim C-Y, Galli G and Wang F 2010 Emerging photoluminescence in monolayer MoS_2 *Nano Lett.* **10** 1271–5

[7] Gutiérrez H R, Perea-López N, Elías A L, Berkdemir A, Wang B, Lv R, López-Urías F, Crespi V H, Terrones H and Terrones M 2012 Extraordinary room-temperature photoluminescence in triangular WS_2 monolayers *Nano Lett.* **13** 3447–54

[8] Tonndorf P *et al* 2013 Photoluminescence emission and Raman response of monolayer MoS_2, $MoSe_2$, and WSe_2 *Opt. Express* **21** 4908–16

[9] Sahin H, Tongay S, Horzum S, Fan W, Zhou J, Li J, Wu J and Peeters F M 2013 Anomalous Raman spectra and thickness-dependent electronic properties of WSe_2 *Phys. Rev.* B **87** 165409

[10] Shaw J C, Zhou H, Chen Y, Weiss N O, Liu Y, Huang Y and Duan X 2014 Chemical vapor deposition growth of monolayer $MoSe_2$ nanosheets *Nano. Res.* **7** 1–7

[11] Li Y, Rao Y, Mak K F, You Y, Wang S, Dean C R and Heinz T F 2013 Probing symmetry properties of Few-Layer MoS_2 and h-BN by Optical Second-Harmonic Generation *Nano Lett.* **13** 3329–33

[12] Malard L M, Alencar T V, Barboza A P M, Mak K F and de Paula A M 2013 Observation of intense second harmonic generation from MoS_2 atomic crystals *Phys. Rev.* B **87** 201401(R)

[13] Kumar N, Najmaei S, Cui Q, Ceballos F, Ajayan P M, Lou J and Zhao H 2013 Second harmonic microscopy of monolayer MoS_2 *Phys. Rev.* B **87** 161403(R)

[14] Zeng H *et al* 2013 Optical signature of symmetry variations and spin-valley coupling in atomically thin tungsten dichalcogenides *Sci. Rep.* **3** 1608

[15] Yin X, Ye Z, Chenet D A, Ye Y, O'Brien K, Hone J C and Zhang X 2014 Edge Nonlinear Optics on a MoS_2 Atomic Monolayer *Science* **344** 488–90

[16] Sutherland R L 2003 *Handbook of Nonlinear Optics* (New York: Dekker)

[17] Shen Y R 2003 *The Principles of Nonlinear Optics* (Hoboken, New Jersey: Wiley)

[18] Boyd R W 2008 *Nonlinear Optics* (Burlington, MA, USA: Academic)

[19] Janisch C, Wang Y, Ma D, Mehta N, Elías A L, Perea-López N, Terrones M, Crespi V and Liu Z 2014 Extraordinary second harmonic generation in tungsten disulfide monolayers *Sci. Rep.* **4** 5530

[20] Wang G, Marie X, Gerger I, Amand T, Lagarde D, Bouet L, Vidal M, Balocchi A and Urbaszek B 2015 Giant enhancement of the optical second-harmonic emission of WSe_2 monolayers by laser excitation at exciton resonances *Phys. Rev. Lett.* **114** 097403

[21] Wagoner G A, Persans P D, Van Wagenen E A and Korenowski G M 1998 Second-harmonic generation in molybdenum disulfide *J. Opt. Soc. Am.* B **15** 1017–21

[22] Karvonen L *et al* 2015 Investigation of second− and third−Harmonic generation in Few−Layer gallium selenide by multiphoton microscopy *Sci. Rep.* **5** 10334

[23] Terrones H *et al* 2014 New first order raman-active modes in few layered transition metal dichalcogenides *Sci. Rep.* **4** 4215

[24] Li H, Lu G, Wang Y, Yin Z, Cong C, He Q, Wang L, Ding F, Yu T and Zhang H 2013 Mechanical exfoliation and characterization of single-and few-layer nanosheets of WSe_2, TaS_2, and $TaSe_2$ *Small* **9** 1974–81

[25] Mead D G and Irwin J C 1977 Long wavelength optic phonons in WSe_2 *Can. J. Phys.* **55** 379–82
[26] Luo X, Zhao Y, Zhang J, Toh M, Kloc C, Xiong Q and Quek S Y 2013 Effects of lower symmetry and dimensionality on Raman spectra in two-dimensional WSe_2 *Phys. Rev.* B **88** 195313
[27] Zhao W, Ghorannevis Z, Amara K K, Pang J R, Toh M, Zhang X, Kloc C, Tan P H and Eda G 2013 Lattice dynamics in mono-and few-layer sheets of WS_2 and WSe_2 *Nanoscale* **5** 9677–83
[28] Zhao W, Ribeiro R M, Toh M, Carvalho A, Kloc C, Castro Neto A H and Eda G 2013 Origin of indirect optical transitions in few-layer MoS_2, WS_2, and WSe_2 *Nano Lett.* **13** 5627–34
[29] Janisch C, Mehta N, Ma D, Elías A L, Perea-López N, errones N and Liu N 2014 Ultrashort optical pulse characterization using WS_2 monolayers *Opt. Lett.* **39** 383–5
[30] Fang H *et al* 2014 Strong interlayer coupling in van der Waals heterostructures built from single-layer chalcogenides *Proc. Natl. Acad. Sci. USA* **111** 6198–202
[31] Bissett M A, Tsuji M and Ago H 2014 Strain engineering the properties of graphene and other two-dimensional crystals *Phys. Chem. Chem. Phys.* **16** 11124–38